Transcriptome analysis in an AEG-1-deficient neuronal HT22 cell line

KUNMEI LIU[1,2*], PANPAN WAN[1*], YUE HUANG[2], BIN WANG[3],
XUEQUAN WANG[4,5], RUI ZHANG[1] and LE GUO[3,6]

[1]Ningxia Key Laboratory of Cerebrocranial Disease; [2]Department of Microbiology and Biochemical Pharmacy,
School of Pharmacy, Ningxia Medical University; [3]Ningxia Key Laboratory of Clinical and Pathogenic Microbiology,
General Hospital of Ningxia Medical University, Yinchuan, Ningxia Hui Autonomous Region 750004; [4]Laboratory of
Cellular and Molecular Radiation Oncology and [5]Department of Radiation Oncology, The Affiliated Taizhou Hospital,
Wenzhou Medical University, Taizhou, Zhejiang 317000; [6]Department of Medical Laboratory, School of Clinical Medicine,
Ningxia Medical University, Yinchuan, Ningxia Hui Autonomous Region 750004, P.R. China

Abstract. Astrocyte elevated gene-1 (AEG-1) is a key regulatory factor of progression in multiple types of tumor and neurodegenerative disease development. AEG-1 is associated with glutamate excitotoxicity due to its reported function of repressing excitatory amino acid transporter 2 expression in astrocytes. Although the function of AEG-1 has been demonstrated in neurological disorders, such as Alzheimer's disease and amyotrophic lateral sclerosis, the underlying mechanism of neuronal AEG-1 function remains unclear. The aim of the present study was to clarify the function and related mechanism of AEG-1 in neurons. A stable AEG-1-deficient HT22 neuronal cell line was constructed using CRISPR/Cas9 gene-editing technology. Reverse transcription-quantitative PCR and western blotting were carried out to analyze the knockdown efficiency of AEG-1-deficient HT22 cell line. RNA Sanger sequencing analysis was performed in AEG-1-deficient HT22 cells and wild-type HT22 cells without knockout (KO). Results from RNA sequencing revealed that AEG-1 modulated neuronal morphology and development by regulating the expression of numerous genes, such as ubiquitin C, C-X-C motif chemokine ligand 1, MMP9, Notch1, neuropilin 1 and ephrin type-A receptor 4. In addition, AEG-1 deficiency impacted several signaling pathways by mediating cell survival differentiation, apoptosis, and migration; this included the TNF-α pathway, the NF-κB pathway, the MAPK signaling pathway, the Notch signaling pathway and Axon guidance. Downregulation in cellular ion homeostasis, including ion channel function and neurotransmitter release, were observed after knocking out AEG-1 expression. Collectively, the present study provides insights into AEG-1-dependent gene regulation and signaling pathway transduction in neurons. The results of the present study may be applied for improving the understanding of AEG-1-associated central nervous system diseases.

Correspondence to: Professor Kunmei Liu, Ningxia Key Laboratory of Cerebrocranial Disease, Ningxia Medical University, 1160 Shengli Street, Yinchuan, Ningxia Hui Autonomous Region 750004, P.R. China
E-mail: lkm198507@126.com

Professor Le Guo, Ningxia Key Laboratory of Clinical and Pathogenic Microbiology, General Hospital of Ningxia Medical University, 1160 Shengli Street, Yinchuan, Ningxia Hui Autonomous Region 750004, P.R. China
E-mail: guoletian1982@163.com

*Contributed equally

Introduction

Astrocyte elevated gene-1 (AEG-1), which is also known as metadherin and lysine-rich carcinoembryonic antigen-related cell adhesion molecule 1 co-isolated, was first observed to be upregulated in brain astrocytes from patients with HIV-induced Alzheimer's disease (1). AEG-1 has been shown to localize to the cell membrane, cytoplasm, endoplasmic reticulum, nucleolus and nucleus in cancer cells (2). At present, the majority of previous studies have focused on the function of AEG-1 in the development and progression of various malignancies such as gastric cancer, breast cancer and malignant glioma (3,4). As an oncogene, AEG-1 has been found to facilitate tumor growth, metastasis, angiogenesis and drug resistance (5,6). In addition, AEG-1 as a key modulator regulates aberrant cellular processes within the central nervous system (CNS), where it is

involved in neurological diseases such as Huntington's chorea, migraine and HIV-induced neurological disorders (7-9).

AEG-1 has differential regulatory effects on astrocytes (AST) and neurons. In AST, AEG-1 causes glutamatergic excitotoxicity by downregulating the activity of the excitatory amino acid transporter 2 (EAAT2) promoter, leading to neuronal cell death in glioma-induced neurodegenerative disease (10). Furthermore, AEG-1 can promote AST activation and hyperplasia induced by brain injury in a mouse model of reactive astrogliosis (11). Silencing AEG-1 expression has also been shown to suppress AST migration and proliferation to wounded areas (11). By contrast, in neurons, downregulation of AEG-1 expression has been shown to reduce the viability of motor neurons in models of amyotrophic lateral sclerosis (ALS), both *in vivo* and *in vitro* (12). In addition, upregulation of AEG-1 expression can protect nigral dopaminergic neurons from injury caused by aberrant apoptotic signaling pathways (13). AEG-1 has also been reported to regulate embryonic neural development (14). Although AEG-1 is evolutionarily conserved in vertebrates, the expression of AEG-1 in CNS cells, including neurons and astrocytes (9,15), has not been previously studied in depth to the best of our knowledge. Therefore, further investigation into the potential role of AEG-1 in neurons and its physiological mechanisms is warranted.

CRISPR/Cas9 technology is a state-of-the-art gene editing method that was originally derived from the prokaryotic adaptive immune system (16). The CRISPR/Cas9 system contains a single guide RNA (sgRNA) molecule and a nucleic acid endonuclease, Cas9. These two components cooperatively cleave the desired sequence in the target DNA at specific locations by forming complementary base pairings. A double-stranded break is subsequently formed (17). In the present study, an AEG-1-deficient neuronal HT22 cell line was constructed using such CRISPR/Cas9 technology. Cell morphology was subsequently observed in AEG-1-deficient cells using light microscope. A list of differentially expressed genes (DEGs) were obtained using RNA-sequencing (RNA-seq) analysis. Functional enrichment analysis on these DEGs was then performed to investigate neuronal AEG-1 function.

Materials and methods

Cell culture. The mouse hippocampal neuronal cells (HT22) were purchased from Jennio Biotech Co., Ltd. The cells were cultured in DMEM (Biological Industries) supplemented with 10% FBS (Biological Industries) and 1% penicillin streptomycin (Beijing Solarbio Science & Technology Co., Ltd.) at 37°C in an incubator with 5% CO_2 for 2 days.

GV392-AEG-1-sgRNA plasmid generation and lentivirus packaging. HT22 cells are highly sensitive to glutamate, have cholinergic neuronal properties and have therefore been proposed to be viable models for studying neurodegenerative diseases (18,19). The present study was designed and performed based on the mouse genome (GRCm39/m29). The full-length cDNA sequence (ATGGCTGCACGAAGCTGG CAGGACGAGCTGGCCCAGCAGGCCGAGGAGGGCTCT GCCCGGCTGCGGGAGTTGCTCTCGGTCGGCCTAGGT TTTCTGCGCACGGAGTTGGGCCTCGACCTGGGGCTA

GAGCCGAAGCGGTACCCGGGCTGGGTGATCCTGGTG GGCACCGGCGCTCTCGGGCTGCTCCTGCTCTTCCTT CTAGGTTACGGCTGGGCCGCGGCTTGCGCCGGCGCC CGCAAGAAGCGAAGGAGCCCGCCCCGCAAACGGGAG GAGGCGGCCCCGCCGACTCCGGCCCCCGACGACCTA GCCCAGCTGAAGAATCTCAGAAGCGAGGAGCAAA AGAAGAAGAACCGGAAGAAGCTTCCTGAAAAGCCCA AACCAAATGGACGGACTGTTGAAGTACCCGAGGATG AAGTTGTTAGAAATCCCCGAAGTATAACTGCAAAAC AAGCACCAGAGACAGACAAGAAAAATGAAAAGTCAA AGAAAAATAAGAAGAAATCAAAGTCAGATGCTAAAG CAGTGCAAAACAGTTCACGCCATGATGGAAAGGAAG TTGATGAAGGAGCCTGGGAAACTAAAATTAGTCACA GAGAGAAACGACAACAGCGTAAACGTGATAAAGTGC TGACTGATTCTGGTTCATTGGATTCAACTATCCCTG GGATAGAAAATATCATCACAGTTACCACCGAGCAAC TTACAACTGCATCATTTCCTGTTGGTTCCAAGAAGA ATAAAGGTGATTCTCATCTAAATGTTCAAGTTAGCA ACTTTAAGTCTGGAAAAGGAGATTCTACACTGCAGG TTTCTTCAAGGCTGAATGAAAATCTTACTGTCAATG GAGGAGGCTGGAGTGAAAAGTCTGTAAAACTCTCCT CACAATTGAGTGAGGAGAAGTGGAACTCTGTCCCAC CTGCTTCTGCAGGCAAGAGGAAAACAGAGCCATCGG CTTGGACTCAAGACACTGGTGACACTAATGCAAATG GGAAAGACTGGGGAAGGAATTGGAGTGATCGCTCAA TATTTTCTGGCATTGGATCTACTGCTGAGCCAGTTTCT CAGTCTACCACTTCTGATTATCAGTGGGATGTTAGC CGTAATCAACCTTATATCGATGATGAATGGTCTGGG TTAAATGGTTTGTCTTCTGCTGACCCTAGCTCAGAC TGGAATGCACCAGCAGAGGAGTGGGGGAACTGGGTA GATGAAGATAGAGCTTCACTTCTGAAGTCCCAGGAA CCAATTTCTAATGATCAAAAGGTTTCAGATGATGAT AAAGAAAAAGGGGAGGGAGCTCTTCCAACTGGAAAA TCTAAAAAGAAAAAGAAGAAAAAGAAGAAGCAA GGGGAAGATAACTCTCACACACAGGACACAGAAGAC CTAGAAAAGGACACTAGAGAAGAGCTTCCAGTGAAT ACCTCAAAAGCCCGACCAAAACAGGAGAAAGCTTGT TCCCTGAAGACCATGAGCACTAGTGACCCAGCTGAA GTACTCATCAAAAATAGCCAGCCTGTCAAGACTCTT CCTCCTGCTATCTCTGCCGAGCCATCTATTACCTTA TCAAAAGGTGACTCTGACAACAGCTCTTCCCAAGTG CCACCGATGTTACAAGACACAGACAAGCCCAAG TCAAATGCTAAGCAAAACAGTGTGCCTCCCTCACAG ACCAAGTCTGAAACTAACTGGGAATCTCCAAAACAA ATAAAAAAGAAGAAAAAAGGCCAGACGGGAAACG TGA) of mouse AEG-1 gene was 3,611 bp and contained 12 transcripts and 12 exons. Exon regions corresponding to the conserved protein sequences were selected for target screening from Feng Zhang Lab Library version 2 (http://www.addgene. org/pooled-library/zhang-mouse-gecko-v2/). Sequences with higher CFD specificity scores and lower number of off-target sites according to the Feng Zhang Lab website (https://zlab. bio/guide-design-resources), were used as main sequences.

The GV392 plasmid (Fig. 1) was purchased from Shanghai GeneChem Co., Ltd. The *BsmB*I site in this GV392 plasmid was selected to be the sgRNA insertion point. The three sets of designed oligonucleotide sequences are listed in Table I. For each of the sgRNA sequences used, 'CACCG' was added to the 5' ends whereas 'AAAC' was added to the 3' end. The GV392 plasmid was subsequently cleaved using
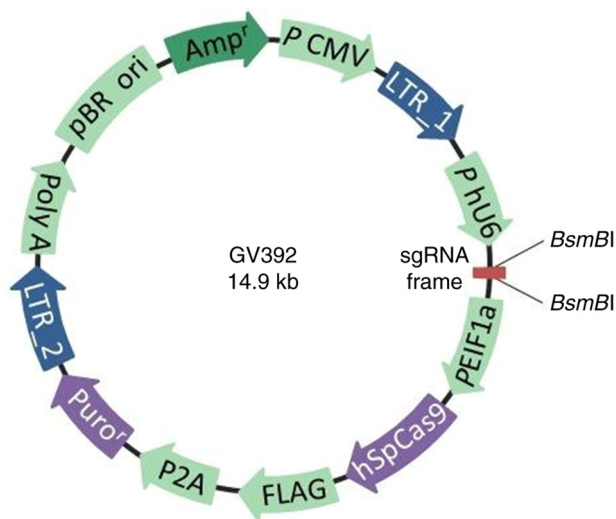
Figure 1. Schematic of the GV392 plasmid. The sgRNA structure is designated to be after the U6 promoter region and contains two *BsmB*I endonuclease sites. sgRNA, single guide RNA.

the restriction endonuclease *BsmB*I (Shanghai GeneChem Co., Ltd.) to obtain the linearized vector. The synthesized sgRNA oligonucleotides (Shanghai GeneChem Co., Ltd.) were then phosphorylated, and annealed at 95°C for 15 min (Shanghai Yuanye Biotech Co., Ltd.) to form double-stranded DNA according to the manufacturer's instructions. T4 DNA Ligase High Concentration Rapid Kit (Fermentas; Thermo Fisher Scientific, Inc.) ligated the linearized GV392 plasmid with the double-stranded sgRNA at 22°C for 3 h, which were then amplified using DH5α-competent E. Coli (Beijing Mei5 Biotech Co., Ltd.).

The GV392-AEG-1 sgRNA lentiviral expression vector was co-transfected with lentivirus packaging helper plasmids (2nd generation; 10 µg lentivirus plasmid used for transfection: 5 µg lentivirus, 3.75 µg packaging and 1.25 µg envelope plasmids) into 293T cells (high sugar DMEM containing 10% FBS, 37°C, 5% CO$_2$; Cell bank of Chinese Academy of Sciences) for lentivirus packaging. Before the virus titer was determined, lentivirus (M-AEG-1-sgRNA-1/M-AEG-1-sgRNA-2/M-AEG-1-sgRNA-3) stock solutions were collected and concentrated by ultracentrifugation at 4,000 x g (4°C) after 48 h at 37°C of transfection.

Generation of AEG-1-deficient HT22 cell lines. The proliferation of the HT22 cells was observed in the presence of 6 and 4 µg/ml puromycin (Fermentas; Thermo Fisher Scientific, Inc.) before the cells were infected with the lentivirus. Cells at logarithmic growth stage were digested with 0.25% trypsin-EDTA solution and inoculated into six-well plates at a density of 1x10^5 cells per well. The cells were infected at 37°C with 50 µl virus M-AEG-1-sgRNA-1 (titer 2x10^8/ml), 50 µl virus M-AEG-1-sgRNA-2 (titer 2x10^8/ml), 50 µl negative control virus (titer 2x10^8/ml) and 33 µl M-AEG-1-sgRNA-3 (titer 3x10^8/ml) at a multiplicity of infection value 50 at the same time, to achieve the optimum infection by each virus. After 3 days of culture in DMEM containing 6 µg/ml puromycin (Beijing Solarbio Science & Technology Co., Ltd.), the puromycin concentration was reduced to 4 µg/ml. Stably infected cells were then inoculated into 96-well plates by trypsin digestion. After 6 h at 37°C, the cells were observed under a light microscope to establish monoclonal cell lines.

Verification of sgRNA activity. To analyze the mutations caused by CRISPR/Cas9, whole genomic DNA was extracted from AEG-1-deficient HT22 cells using PureLink™ Genomic DNA Mini kit (Omega Bio-Tek, Inc.). The DNA fragment was amplified by TB Green® Premix Ex Taq™ II (Tli RNaseH Plus) kit (Takara Bio, Inc.) using AEG-1-sgRNA-specific primers. The forward and reverse primers of AEG-1-sgRNAs are provided in Table II. The PCR cycle was as follows: Initial denaturation at 94°C for 4 min, followed by 35 cycles of denaturation at 94°C for 30 sec, annealing at 48°C for 30 sec, elongation at 72°C for 30 sec and a final extension at 72°C for 12 min. The annealed PCR products were digested with T7 Endonuclease I (New England BioLabs, Inc.), which specifically cleaves mismatched DNA, at 37°C for 1 h. The cleaved DNA fragment was then analyzed using 1.5% agarose gel electrophoresis and visualized by ethidium bromide staining.

Reverse transcription-quantitative PCR (RT-qPCR). Total RNA was collected from normal HT22 cells, negative control virus cells and cells infected with the three M-AEG-1-sgRNA viruses using the TRIzol® reagent (Invitrogen; Thermo Fisher Scientific, Inc.) according to the manufacturer's protocol. The normal HT22 cells were used as the blank control group, whilst the HT22 cells infected with viruses encoding control gRNA were used as the negative control group. RNA purity and concentration were measured using a NanoPhotometer® Spectrophotometer (Implen GmbH). Total RNA was used for the reverse transcriptase reaction with FastKing gDNA Dispelling RT SuperMix kit (Tiangen Biotech Co., Ltd.), the reaction conditions are as follows: Genome removal and reverse transcriptional reaction at 42°C for 15 min, enzyme inactivation process at 95°C for 3 min. To evaluate the expression of blank control group, negative control group and groups infected with the three M-AEG-1-sgRNA viruses at the mRNA level, TB Green® Premix Ex Taq™ II (Tli RNaseH Plus) kit (Takara Bio, Inc.) and CFX96 Real-Time PCR Detection System (Bio-Rad Laboratories, Inc.) were used for PCR amplification. The thermocycling profiles incorporated an initial denaturation at 95°C for 30 sec, followed by 40 cycles of denaturation at 95°C for 5 sec and annealing at 60°C for 30 sec. The sequences of the primers used for qPCR are provided in Table II. The Cq values of qPCR results in each group were converted to $2^{-\Delta\Delta Cq}$ values for comparison (20). The expression levels of each mRNA in the cells were normalized to the level of GAPDH mRNA expression.

Western blotting. The normal HT22 cells, negative control virus cells and cells infected with the three M-AEG-1-sgRNA viruses were lysed using Radio-Immunoprecipitation Assay buffer (100 ml; Jiangsu Keygen Biotech Co., Ltd.) containing phosphatase and proteinase inhibitors at 4°C. The supernatant was then collected from the lysate by centrifugation at 300 x g for 15 min at 4°C. The harvested protein concentrations were measured using the BCA protein quantitation reagent (Nanjing KeyGen Biotech Co., Ltd.). After boiling for 5 min at 95°C, the

Table I. AEG-1 sgRNA oligonucleotides.

Name	Sequence	Exon
M-AEG-1-sgRNA-1	5'-CACCGACTTCAACAGTCCGTCCATT-3' 3'-CTGAAGTTGTCAGGCAGGTAACAAA-5'	2
M-AEG-1-sgRNA-2	5'-CACCGTCATTGGATTCAACTATCCC-3' 3'-CAGTAACCTAAGTTGATAGGGCAAA-5'	3
M-AEG-1-sgRNA-3	5'-CACCGCAAAACAGTTCACGCCATGA-3' 3'-CGTTTTGTCAAGTGCGGTACTCAAA-5'	4
Negative control sgRNA	5'-CACCGCGCTTCCGCGGCCCGTTCAA-3' 3'-CGCGAAGGCGCCGGGCAAGTTCAAA-5'	

AEG-1, astrocyte elevated gene-1; sgRNA, single guide RNA.

Table II. Primer list.

Name	Direction	Sequence
Primers of M-AEG-1-sgRNA-1	Forward	5'-TTTCATTGTTGTATATGTTATTTCC-3'
	Reverse	5'-AGACTACACTCTTATTAACCATGAA-3'
Primers of M-AEG-1-sgRNA-2	Forward	5'-CTTTTATACCACACACCTCAGTTTA-3'
	Reverse	5'-AGTTGTCAGTTTCATACATTTCATT-3'
Primers of M-AEG-1-sgRNA-3	Forward	5'-TCAGCACAAAGTTAGCAGTTCAAAA-3'
	Reverse	5'-TCAGGAGCCTGGGAAACTAAAATTA-3'
AEG-1 qPCR primer	Forward	5'-CCGCAAGAAGCGAAGGAGC-3'
	Reverse	5'-CCGTCCATTTGGTTTGGGCT-3'
GAPDH qPCR primer	Forward	5'-AGGCCGGTGCTGAGTATGTC-3'
	Reverse	5'-TGCCTGCTTCACCACCTTCT-3'

AEG-1, astrocyte elevated gene-1; sgRNA, single guide RNA; qPCR, quantitative PCR.

total protein (50 μg) was resolved using 10% SDS-PAGE gels and transferred onto polyvinylidene difluoride membranes (MilliporeSigma). The membranes were blocked in 5% skimmed milk for 1 h at room temperature and then probed with the anti-AEG-1 antibody (cat. no. 13860-1-AP; 1:1,000; ProteinTech Group, Inc.) or the anti-GAPDH antibody (cat. no. GTX100118; 1:1,000; GeneTex, Inc.) overnight at 4˚C, before being incubated with the secondary antibody (Dylight 800; goat anti-rabbit IgG; 1:2,000; cat. no. A23920; Abbkine Scientific Co., Ltd.) for 1 h at room temperature. Finally, the membranes were developed using ECL reagents (Pierce; Thermo Fisher Scientific, Inc.) and visualized using the full-automatic chemiluminescence imaging analysis system (Bio-Rad Laboratories, Inc.). The integrated band densities were measured using ImageJ v1.8.0. software (National Institutes of Health).

The group of cells (those transfected with the M-AEG-1-sgRNA-3) with the highest knockdown effect were screened based on the western blotting and qPCR results. Genomic DNA of the AEG-1-KO monoclonal cell line was extracted and amplified by AEG-1 specific primers (methods as aforementioned). The PCR products were then purified using MiniBEST DNA Fragment Purification Kit Ver.4.0 (Takara Bio, Inc.) and ligated to a pMD19-T vector using pMD™ 19-T Vector Cloning Kit (Takara Bio, Inc.). The product was transformed into TOP10 competent cell (Shanghai GeneChem Co., Ltd.) and positive clones were obtained by colony PCR. The positive bacterial colonies were selected to extract plasmids for Sanger sequencing analysis.

RNA quantification and library construction. RNA purity and concentration was checked using a NanoPhotometer spectrophotometer (Implen, Inc.) and Qubit® RNA Assay kit (cat. no. Q10210) in combination with the Qubit 2.0 Fluorometer (both Thermo Fisher Scientific, Inc.). RNA integrity was assessed using an RNA 6000 Nano Kit with a Bioanalyzer 2100 system (both Agilent Technologies, Inc.).

For the RNA sample preparations, sequencing libraries were generated with a total amount of 993 mole RNA per sample using the NEBNext® Ultra™ RNA Library Prep Kit for Illumina® (cat. no. E7530L; New England BioLabs, Inc.). Briefly, the mRNA was separated from total RNA samples using magnetic beads coupled with oligo (dT) and fragmented using divalent cations in 5X NEBNext First Strand Synthesis Reaction Buffer (New England Biolabs, Inc.) according to the manufacturer's protocol. Next, the mRNA was reverse

transcribed to synthesize double-stranded complementary DNA (cDNA) using Moloney Murine Leukemia Virus Reverse Transcriptase (New England BioLabs, Inc.) with random hexamer primers. The 3' ends of the cDNA were added to the base A and an NEBNext Adaptor (New England BioLabs, Inc.) with a hairpin loop structure to prepare for hybridization. The cDNA target fragments were purified with the AMPure XP system (cat. no. A63381; Beckman Coulter, Inc.) to select fragments 200 bp in length with the direction of 5'-3'. Subsequently, 3 μl USER Enzyme (New England Biolabs, Inc.) was used with size-selected, adaptor-ligated cDNA at 37°C for 15 min followed by 5 min at 95°C before PCR. PCR was performed with Phusion High-Fidelity DNA polymerase, Universal PCR primers and Index (X) Primer. Finally, the PCR products were purified also using the AMPure XP system and used to obtain a sequencing library. The library quality was assessed using the Bioanalyzer 2100 system (Agilent Technologies, Inc.) and the effective concentration (>2 nM) of the library was accurately quantified using RT-qPCR.

Clustering and sequencing. Indicator-coded samples were clustered on the cBot Cluster Generation System using TruSeq PE Cluster Kit v3-cBot-HS (cat. no. PE-401-3001; Illumina, Inc.). Sequencing was then performed via the HiSeq X Ten System (cat. no. SY-412-1001; Illumina, Inc.).

Data analysis. Clean data (clean reads) of fastq format were first obtained by excluding adapters, ploy-N and low-quality reads (reads for which >50% of the read length had a Phred quality value ≤20) from the original data (raw reads) through in-house Perl Script (fastq v1.0, the parameter was fastq-g-q 5-u 50-n 15-l 150; https://www.novogene.cn/) programming. The Q20, Q30 and guanine-cytosine content of the clean data were calculated simultaneously using fastp (v0.19.4) software (Shenzhen Haplox Biotech Co., Ltd.). High-quality clean reads which passed through the described above filtering steps were used for downstream analysis and mapped to the mouse reference genome (accession no. GRCm39) using HISAT2 v2.0.5 (http://daehwankimlab.github.io/hisat2/). The clean reads were compared with reference genes (accession no. GRCm39) (https://www.ncbi.nlm.nih.gov/assembly/GCF_000001635.27/) using TopHat2 v2.0.0 (http://ccb.jhu.edu/software/tophat/index.shtml).

Gene expression characterization and differential gene expression analysis. Gene expression levels were estimated using featureCounts v1.5.0-p3 (http://subread.sourceforge.net/). The expected number of fragments per kilobase of transcript per million fragments mapped (21) was calculated using the Cufflinks software v2.0.1 (http://cufflinks.cbcb.umd.edu/) based on the length of each gene. EdgeR R package v3.18.1 (http://www.bioconductor.org/) (22) was employed to evaluate differential gene expression analysis between different groups (two biological replicates per condition) (23). The DESeq2 package v1.16.1 (http://www.bioconductor.org/packages/release/bioc/html/DESeq2.html) was used to identify differentially expressed genes. The method of Benjamini and Hochberg (24) was used to adjust for the resulting P-values to exclude false positive results. Genes were assigned to be differentially expressed by DESeq2 with adjusted P-values <0.05 and log$_2$ fold change >0.

Gene ontology (GO) analysis and Kyoto encyclopedia of genes and genomes (KEGG) pathway analysis. GO (25) analysis used |log$_2$ fold change|>0 and padj <0.05 as threshold (padj stands for corrected P-value), and performed on the DEGs using the clusterProfiler R package (V3.4.4) (26). KEGG (27) is a database resource for understanding the advanced functions and utilities of biological systems at the molecular level. The clusterProfiler R package was used to analyze the statistical enrichment of DEGs in KEGG pathways (http://www.genome.jp/kegg/), with a Benjamini-Hochberg-adjusted P-value cutoff of <0.05.

Protein-protein interaction (PPI) network analysis. The PPI network of DEGs was analyzed using the STRING database (v11.5; ELIXIR; https://string-db.org) (28), a pre-computed database of known and predicted protein interactions, including direct (physical) and indirect (functional) associations derived from co-expression, co-occurrence, genomic context, gene fusion, high-throughput experiments and text mining. The protein networks were then presented using Cytoscape software v3.7.1 (http://www.cytoscape.org/) with a confidence level of 0.7 and calculation conditions were P<0.05 and no non-coding RNAs allowed. The 'Molecular Complex Detection (MCODE)' plugin for Cytoscape was used to analyze network modules (29). The parameters of densely connected regions or clusters in the co-expression network were set as follows: 'Degree cut-off'=2, 'k-core'=2 and 'max. depth'=100. The 'cytoHubba' plugin for Cytoscape was used to screen for hub genes (30) under the following conditions: 'Top10 node(s)' ranked by 'Degree'.

Statistical analysis. Values were presented as the mean ± standard error of the mean (n≥3). All statistical analysis and graph illustrations were performed using Prism V8.0 (GraphPad Software, Inc.). One-way ANOVA analysis was assessed the differences between multiple groups. Dunnett's test was used for all comparisons with a negative control group. P<0.05 was considered to indicate a statistically significant difference.

Results

GV392-AEG-1-sgRNA plasmid construction and sgRNA activity validation. The inserts of the GV392-AEG-1-sgRNA plasmid with the three AEG-1-sgRNA sites were validated by Sanger sequencing (Fig. 2A). To verify the efficiency of AEG-1-sgRNAs, both insertion and deletion mutations were evaluated in the genomic DNA sequence of AEG-deficient neuronal HT22 cells. SgRNA directs Cas9 protein to bind to the target sequence, Cas9 protein is a nuclease that creates a cut at the target sequence site and DNA repair occurs by mutation (31). All three AEG-1-sgRNAs effectively caused mutations in the specific sites with 89, 94 and 99% efficiency for M-AEG-1-sgRNA-1, M-AEG-1-sgRNA-2 and M-AEG-1-sgRNA-3, respectively (Fig. 2B). The number of protrusions was reduced in AEG-1-deficient neuronal HT22 cells compared with normal HT22 cells, especially in the cell group transfected with the M-AEG-1-sgRNA-3 virus (Fig. 2C).
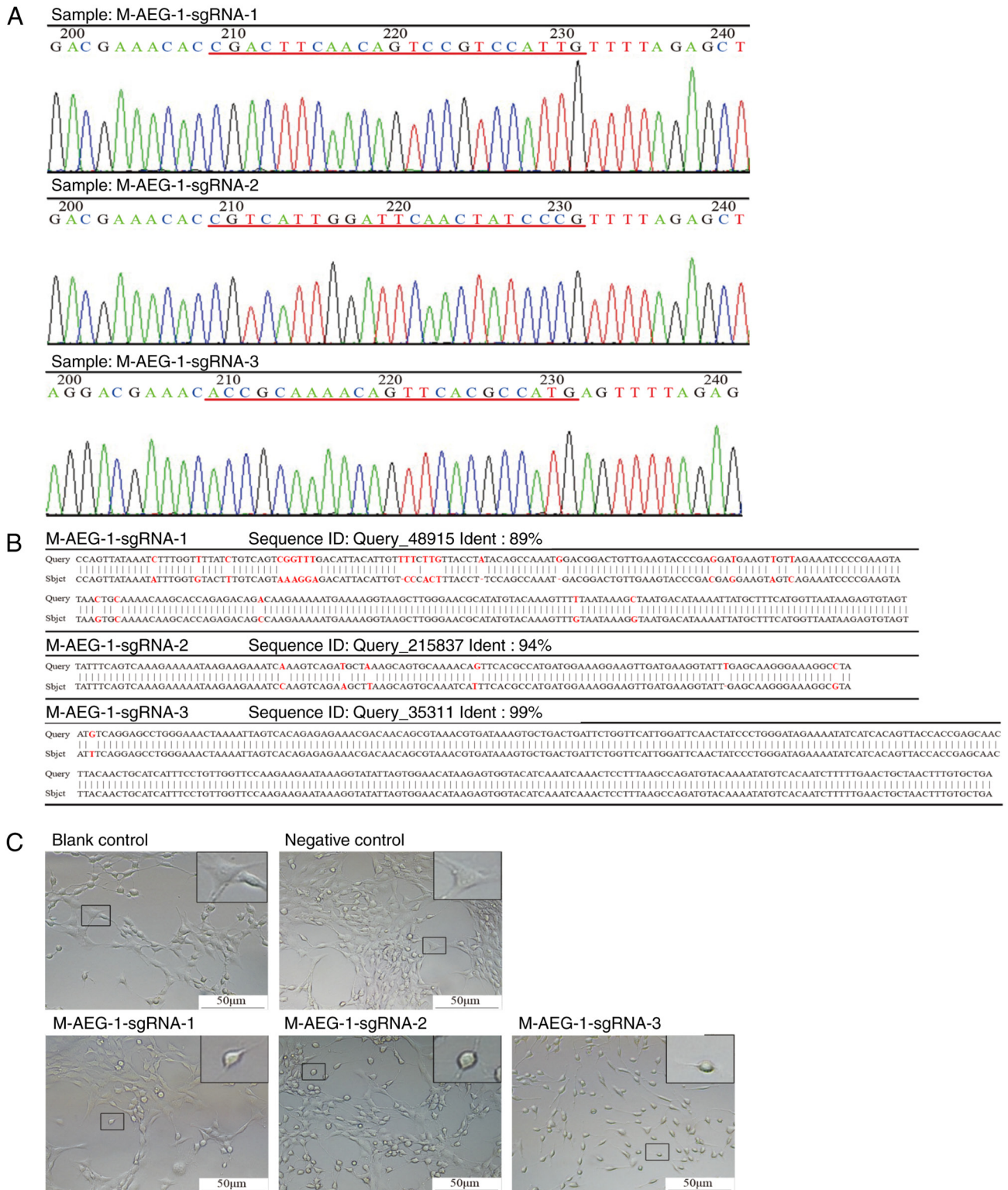
Figure 2. Construction of GV392-AEG-1-sgRNA plasmids and stable AEG-1 knockdown in HT22 cell lines. (A) Sequencing demonstrated that the sgRNA had been correctly inserted into the GV392 plasmid. (B) The sequencing results from the three groups of PCR products showing that there were mutations and deletions at different levels, which was in line with the experimental design (the PCR product of the validation primer contained the target sequence site, and the mutation of the PCR product indicated that the designed sgRNA couldmutate the target sequence). (C) Morphology of HT22 cells after infection with virus M-AEG-1-sgRNA-1, M-AEG-1-sgRNA-2, M-AEG-1-sgRNA-3 or the negative control virus in 10x bright-field (scale bar, 50 μm). The blank control was HT22 cells without viruses. Rectangles indicate individual cells for comparison. Microscope observation revealed that AEG-1 knockdown in HT22 cells exhibited changes in cell morphology. AEG-1, astrocyte elevated gene-1; sgRNA, single guide RNA.

Verification of AEG-1 knockdown. qPCR and western blot analysis were performed to select for AEG-1-deficient HT22 cell lines with the highest knockdown efficiency. As mentioned above, SgRNA directs Cas9 protein to bind to the target sequence, Cas9 protein is a nuclease that creates a cut at the target sequence site and DNA repair occurs by mutation.

Table III. RNA-sequencing data statistics.

Groups	Clean reads	Clean bases, G	GC content, %	% ≥ Q20	% ≥ Q30
N_con_1	58731670	8.81	53.91	97.91	94.15
N_con_2	59762786	8.96	51.26	97.52	93.23
N_con_3	57048890	8.56	50.90	97.84	93.93
AEG-KO_1	70543436	10.58	50.94	97.86	94.01
AEG-KO_2	66312428	9.95	51.86	97.81	93.89
AEG-KO_3	56271306	8.44	51.61	97.85	93.97

N_con, negative control; AEG-1, astrocyte elevated gene-1; KO, knock-out; GC, guanine-cytosine.
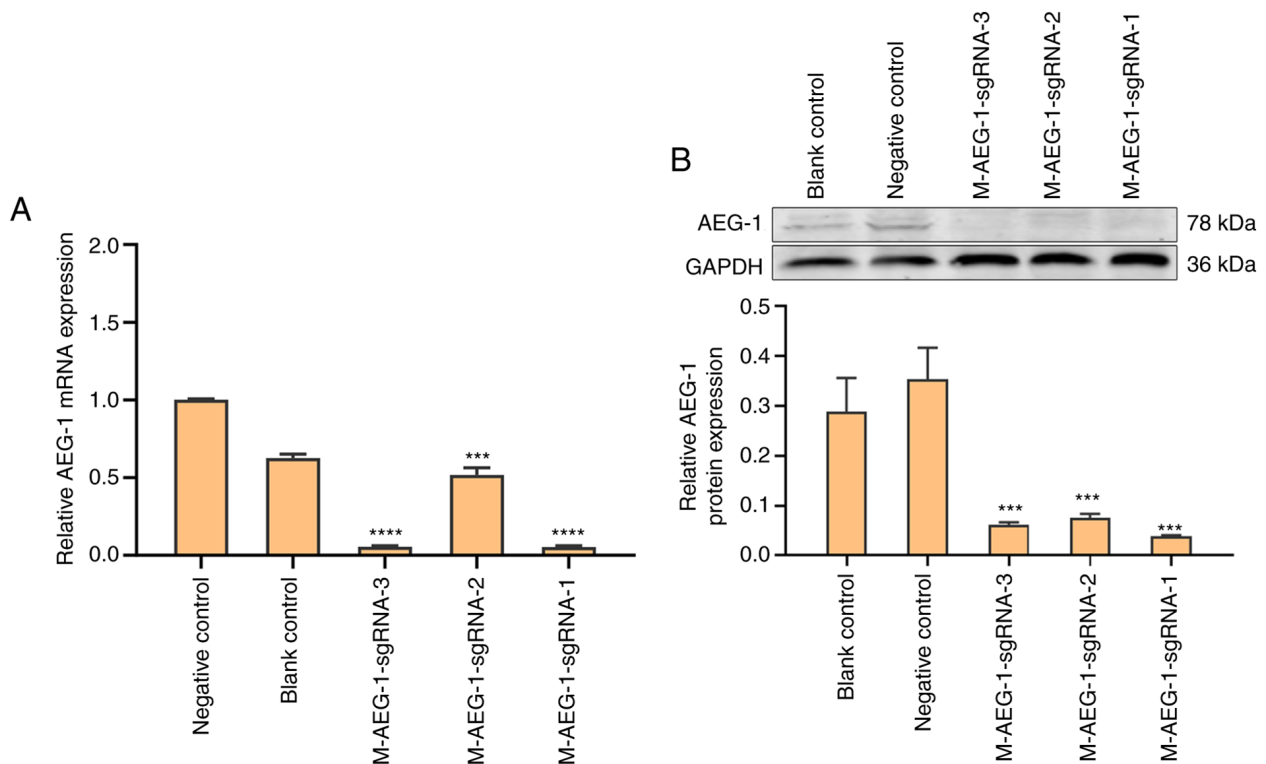

Figure 3. Expression of AEG-1 in virus-infected cells. (A) The mRNA levels of AEG-1 in the HT22 cell line infected with M-AEG-1-sgRNA-1/2/3 were reduced. ****P<0.0001 and ***P<0.001 vs. negative control. (B) The protein expression level of AEG-1 was lower in the AEG-1-sgRNA virus-infected cell group compared with that in the negative control group. ***P<0.001 vs. negative control. Data are presented as the mean ± SEM (n=3). AEG-1, astrocyte elevated gene-1; sgRNA, single guide RNA.

The results suggest that all three M-AEG-1-sgRNA cell lines showed significant reductions in AEG-1 expression compared with that in the negative control group, with the highest knockdown efficiency in the M-AEG-1-sgRNA-1 cell line (Figs. 3A and B and S1). Therefore, the M-AEG-1-sgRNA-1 group was selected for subsequent transcriptomic analysis. The higher AEG-1 expression in the negative control compared with the blank control may have been the effect of the viral empty vector on the AEG-1 virus.

RNA-seq analysis and reference gene sequence comparison. An average of 58,514,448 clean reads of differentially expressed mRNAs were obtained in the control group, whilst an average of 64,377,723 clean reads were obtained in the AEG-1-KO group. Sequencing quality information is listed in Table III. The clean reads were compared with reference genes using TopHat2 v2.0.0. The comparison efficiency refers to the percentage of mapped reads in clean reads, and the comparison efficiency was 95.91% in the control group and 96.14% in the AEG-1-KO group (Table SI).

Gene expression identification and DEG analysis. Variations in gene expression were presented in volcano plots by comparing the control and AEG-1-KO groups. Genes with similar expression patterns were categorized and clustered into hierarchical clustering heat maps. A total of 1,747 DEGs were screened based on the selection criteria of |log2 fold change|>0 and P<0.05. Among the 1,747 DEGs, 758 genes were upregulated and 989 genes were downregulated in the AEG1-KO group compared with the control group (Fig. 4A and B).
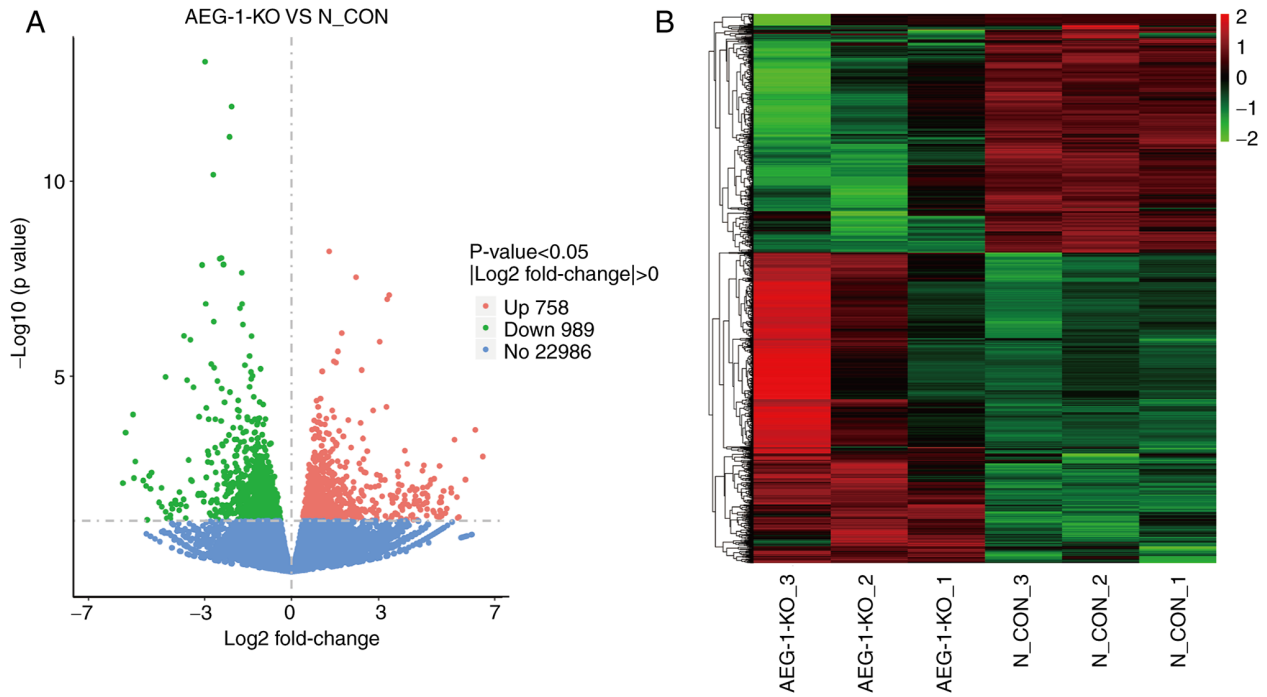
Figure 4. Schematic diagram of differential gene distribution. P<0.05 and |log2 fold change|>0 was used as the selection criteria for differential genes. A total of 1,747 differentially expressed genes showed significant changes. (A) Volcano map. (B) Heat map. The color in each square was the value obtained by normalizing the rows of gene expression data. In horizontal comparison, red indicated higher expression levels, whereas green represented lower expression levels. AEG-1, astrocyte elevated gene-1; KO, knockout; N_CON, negative control.
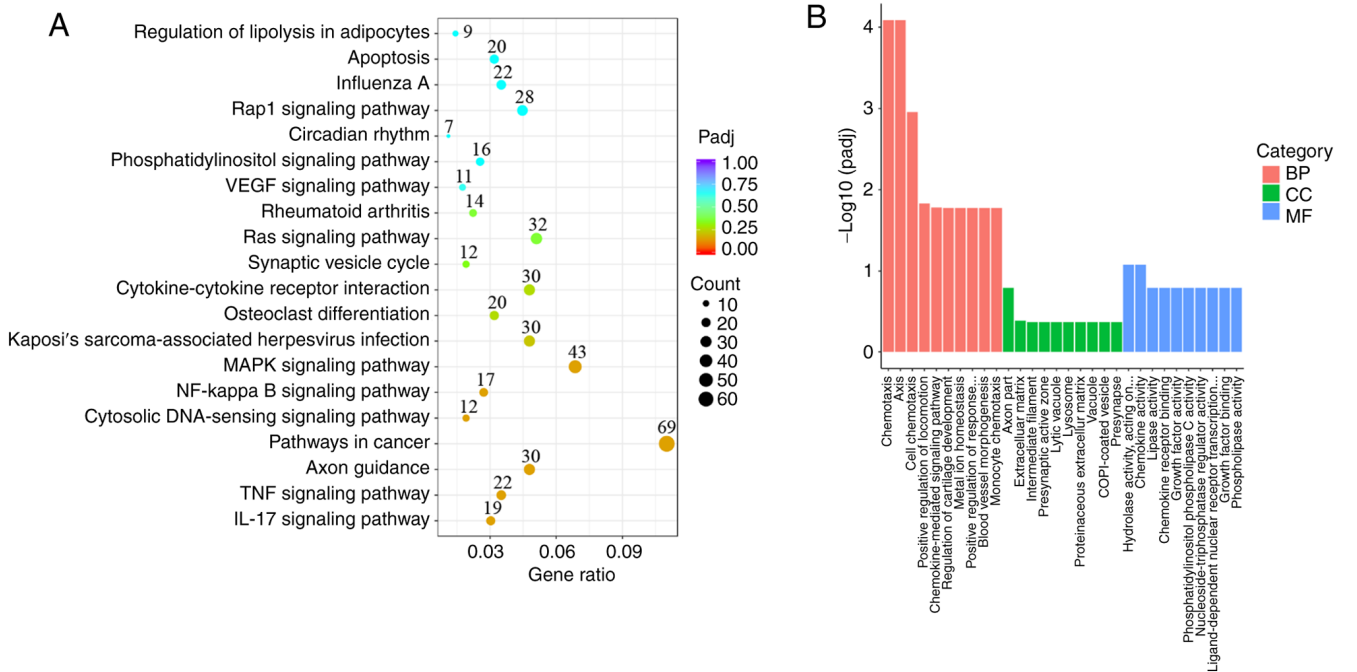

Figure 5. KEGG and GO functional enrichment analysis of DEGs after AEG-1 knockdown. (A) KEGG pathway enrichment analysis showed the top 20 pathways. The abscissa in the figure was the ratio in the number of DEGs annotated to the KEGG pathway to the total number of the genes. The ordinate was the KEGG pathway. The size of the dots represents the number of genes annotated to the KEGG pathway. The color from red to purple represented the significance of enrichment. (B) GO annotation of the enrichment scores of DEGs. The abscissa was the GO Term and the ordinate was the significance level of GO Term enrichment. Different colors represented the three GO sub-categories: BP, CC and MF. KEGG, Kyoto Encyclopedia Gene and Genomic; GO, Gene Ontology; DEGs, differentially expressed genes; BP, biological processes; CC, cell composition; MF, molecular function; Padj, adjusted P-value.

KEGG pathway analysis and GO analysis on DEGs. KEGG pathway analysis and GO analysis were performed to uncover the potential roles of the selected DEGs following AEG-1 knockdown. The selected DEGs were particularly enriched in 20 signaling pathways (Fig. 5A). The top five enriched pathways were 'Axon guidance', 'Pathways in
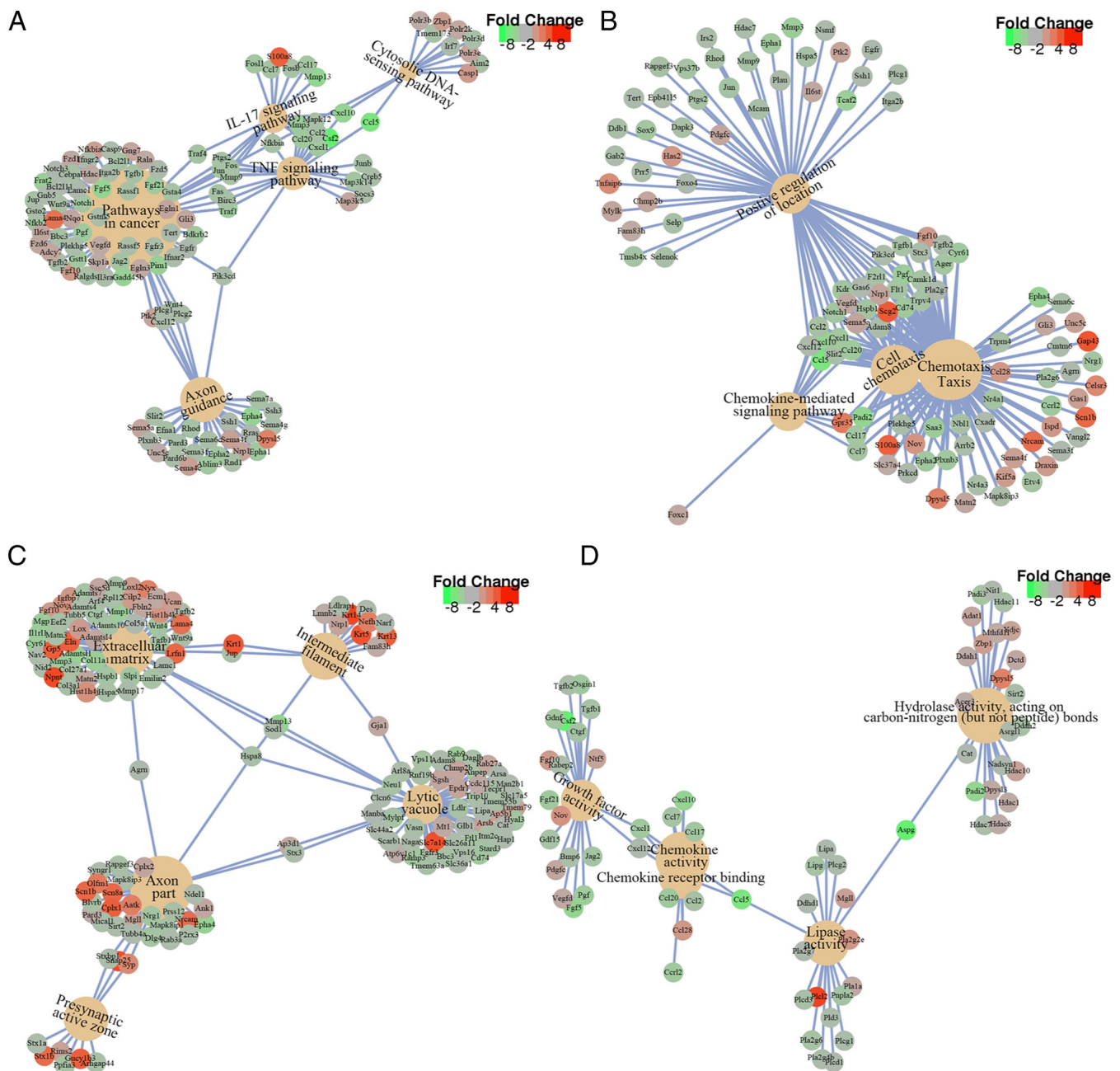
Figure 6. Top five KEGG pathways and GO terms. (A) The KEGG pathways and associated gene networks. The orange nodes represent the KEGG pathway. Nodes of other colors represent the differential genes enriched in each KEGG pathway and the shade of color represent the fold change of each differential gene. The size of the orange node was proportional to the number of differential genes enriched in the pathway. The top five most significant GO terms and associated gene networks in (B) biological processes, (C) cell composition and (D) molecular function. KEGG, Kyoto Encyclopedia Genes and Genomes; GO, Gene Ontology.

cancer', 'TNF signaling pathway', 'IL-17 signaling pathway' and 'Cytosolic DNA-sensing signaling pathway', which are closely associated with inflammation, cell proliferation and differentiation (Figs. 5A and 6A) (32-34). GO analysis showed that the DEGs were mainly enriched in terms of biological processes (BP), cell composition (CC) and molecular function (MF) (Fig. 5B). Within BP, DEGs were particularly enriched in 'chemotaxis', 'taxis', 'cell chemotaxis', 'positive regulation of locomotion' and 'chemokine-mediated signaling pathway' (Figs. 5B and 6B). Within CC, DEGs were refined in 'axon part', 'extracellular matrix', 'intermediate filament', 'presynaptic active zone' and lytic vacuole'

(Figs. 5B and 6C). Within MF, DEGs were primarily enriched in 'hydrolase activity', 'carbon-nitrogen (except peptide) bonds', 'chemokine activity', 'lipase activity', 'chemokine receptor binding' and 'growth factor activity' (Figs. 5B and 6D).

Protein-protein interaction network analysis and hub gene selection. Protein interactions networks of DEGs were analyzed using the STRING database. DEGs formed a complex network containing 221 nodes and 395 degrees with a higher degree of connectivity (Fig. 7A). By using the MCODE application within the Cytoscape software,
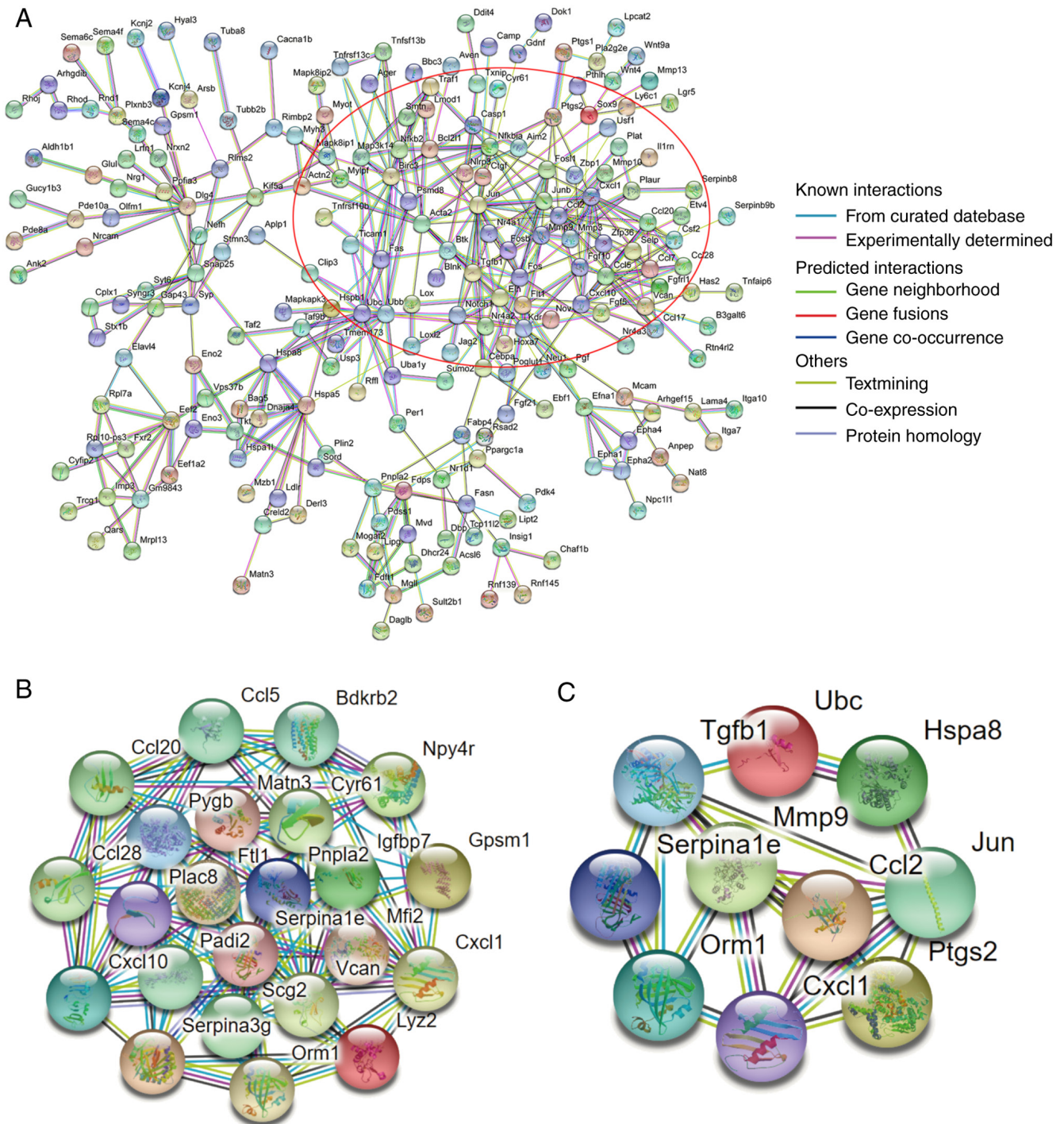
Figure 7. Alignment of the differentially expressed genes to the STRING protein interaction network. (A) A total of 221 nodes and 395 interaction relationships were selected. The network calculation conditions were P<0.05 and no non-coding RNAs allowed. The confidence score for all protein interaction calculations was set to high (>0.7). The red circle highlights most important part of this network. (B) A sub-network containing 23 genes and 81 edges. (C) The hub genes map associated with astrocyte elevated gene-1, generated by the protein-protein interaction network and according to the RNA-sequencing database results.

significant modules in the PPI network were detected. There was a top module in this network, which contained 23 node genes and 81 interaction pathways (Fig. 7B). Filtered by degree calculation, 10 hub genes were obtained: Ubiquitin C (UBC), C-X-C motif chemokine ligand 1 (CXCL1), matrix metallopeptidase 9 (MMP9), orosomucoid 1, JUN, TGFβ1, SERPINA1E, heat shock protein family A (Hsp70) member 8, CC motif chemokine ligand 2 and prostaglandin-endoperoxide synthase 2 (Fig. 7C).

Characterization of genes associated with neurogenesis and ion homeostasis. Certain DEGs such as neuropilin 1 (NRP-1) and Notch1 were involved in axon guidance, cell migration, neuronal differentiation, regulation of exocytosis and formation of certain neuronal circuits (Fig. 8A), suggesting that the reduced expression of these DEGs greatly affected the development of the nervous system process. In addition, 30 DEGS associated with ion homeostasis were categorized, especially the genes of ion channels such as calcium, sodium
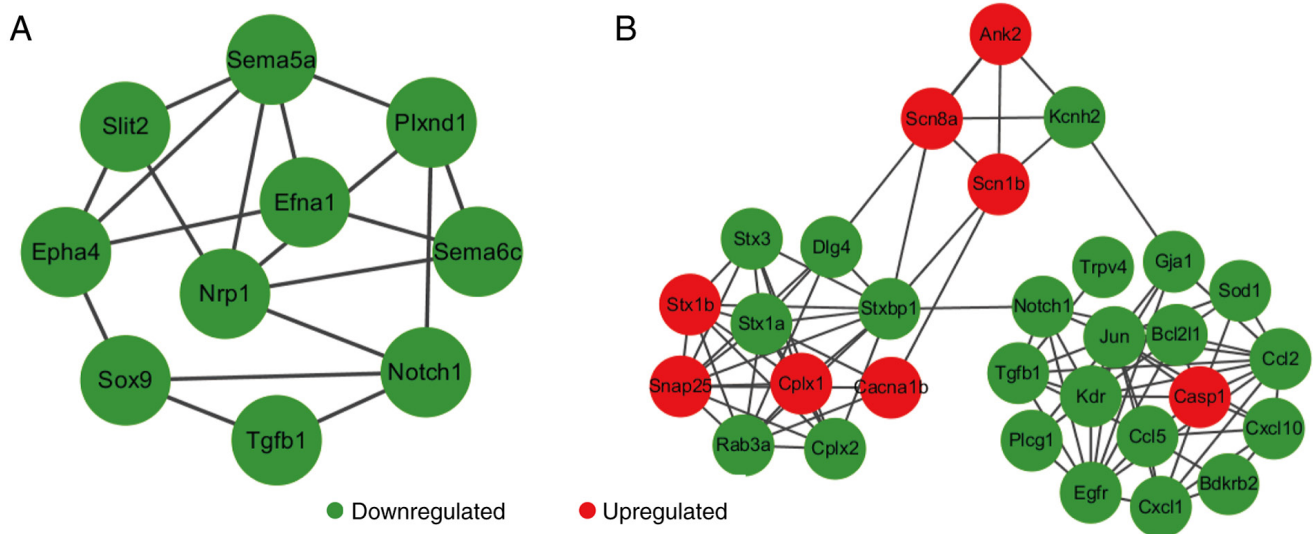
Figure 8. Protein-protein interaction networks of genes associated with neurogenesis and ion homeostasis identified by the Cytoscape software. (A) Changes in neurogenesis-associated genes after AEG-1 knockdown. A network of genes downregulated are shown. (B) Changes in the expression of genes associated with ion homeostasis, including eight genes that were upregulated and 22 genes that were downregulated.

and potassium channels and neurotransmitter release, including calcium voltage-gated channel subunit α1 B, sodium voltage-gated channel β subunit 1, potassium voltage-gated channel subfamily h member 2, synaptosome associated protein 25, syntaxin 3 and RAB3A (Fig. 8B). These results suggest that AEG-1 deficiency contributes to the regulation of neurotransmitter release. Therefore, AEG-1 may serve a potential role in the synaptic function of neuronal systems.

Discussion

In recent years, the CRISPR/Cas9 system has greatly promoted site-specific mutagenesis and has broad applications such as gene function identification, disease modeling, gene therapy and immunotherapy (35-37). The CRISPR/Cas9 system only requires the function of sgRNAs, which is less complex and more cost-effective to design compared with alternative methods of knocking out or editing genes, such as zinc finger nuclease and transcription activator-like effector nuclease (38). In particular, CRISPR/Cas9 is a reliable method for knocking down the expression of the desired gene (39). HT22 is a widely used hippocampal neuron cell line that has been extensively studied in the context of a variety of nervous system diseases, such as Alzheimer's disease and Parkinson's disease (18,19). In the present study, although the viability of the HT22 cells was not assessed prior to the experiments, the cells could reach 80% confluence after 2 days of culture, which indirectly suggest that the HT22 cell line had maintained their viability. However, testing the viability of this cell line before viral infection would render the present study more rigorous. Therefore, this part of the experiment should be performed in further studies. In the present study, AEG-1-deficient HT22 cell lines were generated using the CRISPR/Cas9 technology. Validation using qPCR and western blotting showed that M-AEG-1-sgRNA-3 achieved high efficiencies of knocking down AEG-1 expression, which provided the opportunity to study AEG-1 function in the neuronal cells *in vitro*.

AEG-1 is a potent oncogene that has been reported to contribute to distinct processes during HIV-1 infection, glutamate regulation and tumorigenesis at the time of its initial cloning and identification (10). AEG-1 has also been proposed to contribute significantly to neurodegenerative diseases and is a potential therapeutic target (40,41). Huntington's disease (HD) is a fatal progressive neurodegenerative disorder. In an immortalized striatal cell model of HD and brain tissues from individuals with HD, immunohistochemical analysis has demonstrated that AEG-1 expression was upregulated (15), suggesting that there may be an association between AEG-1 and the pathogenesis of HD. Furthermore, the role of AEG-1 in another neurodegenerative disease, ALS, has also been investigated (12). Upregulation of neuronal AEG-1 can protect nigral dopaminergic neurons from mSOD1-induced cell injury and has been associated with improvements in the viability of motor neurons of the mutant SOD1 in an ALS model (12). In addition, previous findings on the role of AEG-1 in oxidative stress, a common link in multiple CNS pathologies, revealed that AEG-1 likely regulates a number of neurodegenerative processes such as atherosclerosis, stroke and aging (42,43). Although AEG-1 remain poorly explored in the context of neurodegenerative diseases, AEG-1 has been previously implicated in endoplasmic reticulum/nucleus stress (7) and glutamate-mediated neurotoxicity, highlighting its plausible role in other neurodegenerative diseases. In the present study, the gene expression profile after AEG-1 expression was knocked down was studied to elucidate the possible regulatory mechanism of neuronal AEG-1 in neurodegenerative diseases.

According to the GO analysis results, AEG-1 was mainly involved in neuronal morphology and synaptic development. Subcellular compartments of neurons include dendrites, axons and synapses, all of which can impact the formation of neuronal circuits and functional transmission of electrical information (44). Defects in the formation or development of dendrites, axons and synapses can lead to a number of diseases, such as Alzheimer's disease and epilepsy (45). KEGG pathway

analysis indicated that several pathways were impacted after AEG-1 knockdown. The IL-17 and the NF-κB signaling pathways, which are involved in inflammation (32-34), were altered. In addition, the MAPK, RAS and phosphatidylinositol signaling pathways were changed, which are involved in cell proliferation and differentiation (46-48). The other regulatory pathways, such as 'axon guidance and synaptic vesicle cycle', were validated further to analyze the relationship between AEG-1 knockdown and neuronal morphology development.

Numerous DEGs were identified that associated with neurogenesis and axonogenesis. Bioinformatics analysis revealed that NRP-1 is a key gene that relies on AEG-1 function (Fig. 8A). Chemorepulsant activity of semaphorins is mediated by NRP-1 (49). It is also important for the pre-target sorting of axon fasciculation in the peripheral nervous system (50). Therefore, AEG-1 potentially mediates axonogenesis by regulating NRP-1 function. Notably, Notch1 was categorized in the DEGs that was AEG-1-dependent (Fig. 8A).

As a member of the Notch signaling pathway, Notch1 is involved in the proliferation and apoptosis of different cell types in a variety of organisms (51). In particular, neurogenesis and development of the dentate gyrus have been associated with Notch1 expression (52). Loss of Notch1 expression in the dentate gyrus leads to cognitive and emotional impairments; the present study revealed that deletion of AEG-1 downregulated Notch1 suggesting that AEG-1 can regulate neurogenesis through regulating Notch1 (53). Since ephrin-A5/EphA4 interaction is considered to be associated with neuron generation *de novo*, microvascular remodeling and spontaneous recurrent seizures (54,55), EphA4 and slit guidance ligand 2 are also potential genes regulated by AEG-1 in nervous system diseases. In addition, 30 DEGs were involved in ion channels, including calcium, sodium and potassium channels (Fig. 8B). Calcium efflux in neurons is essential for synaptic signaling processes, neuronal energy metabolism and neurotransmission (56). It was revealed that that AEG-1 deletion disturbed genes related to the calcium signaling pathway, which may indirectly affect the development of the nervous system.

Furthermore, 10 hub genes were screened from the DEGs that can potentially serve important roles in biological process of the neuron. UBC, CXCL1 and MMP9 were among the top 10 hub genes based on 'Top10' node(s) ranked by 'Degree'. UBC participates in ubiquitination through forming a polyubiquitin chain and labeling proteins (57). A variety of neurological, skeletal and muscular disorders have been associated with the downregulation of UBC (58). By contrast, CXCL1 is a chemokine that has been reported to improve both nociceptor and central sensitization through biding with C-X-C motif chemokine receptor 2 (59). CXCL1 is a potential target for novel analgesic drugs (60). MMP9 is a member of the endopeptidase family that promotes tissue remodeling by degrading extracellular matrix components (61). Therefore, AEG-1 deficiency may be able to regulate the development of neurological disorders through multiple targets.

In summary, RNA-seq analysis was used to identify potential genes and pathways that are regulated by AEG-1 expression upstream of neuronal function. AEG-1 is considered to be a key protein in nervous system development by regulating signaling pathways and gene expression. The present study found that AEG-1 knockdown disrupted the function of proteins involved in intracellular signal transduction, ion channels and neurotransmitter release. There are two major limitations in the present study that should be addressed in future studies. The present study focused on the RNA-seq analysis of DEGs and functional enrichment after AEG-1 knockdown. However, the DEGs were not validated using qPCR. In addition, this neuronal cell line cannot be viewed as a perfect representation of primary neurons. Despite these limitations, the present study provided novel findings into potential genes and pathways that were regulated by AEG-1 expression upstream of neuronal function through RNA-seq analysis. Validation of the DEGs by qPCR and continued exploration of the exact functional mechanism of AEG-1 in HT22 cells should be the aim of future studies.

Availability of data and materials

The datasets generated and/or analyzed during the current study are available in the NCBI repository (https://www.ncbi.nlm.nih.gov/sra/PRJNA836164).

Authors' contributions

KL, PW and YH analyzed the RNA-sequencing data and wrote the manuscript. BW constructed the AEG-1 knockout cell line. XW and RZ performed data analysis and manuscript review. LG conducted the study design and supervised the study. All authors have read and approved the final manuscript. KL and LG confirm the authenticity of all the raw data.

Ethics approval and consent to participate

Not applicable.

Patient consent for publication

Not applicable.

Competing interests

The authors declare that they have no competing interests.

References

1. Su ZZ, Kang DC, Chen Y, Pekarskaya O, Chao W, Volsky DJ and Fisher PB: Identification and cloning of human astrocyte genes displaying elevated expression after infection with HIV-1 or exposure to HIV-1 envelope glycoprotein by rapid subtraction hybridization, RaSH. Oncogene 21: 3592-3602, 2002.
2. Thirkettle HJ, Girling J, Warren AY, Mills IG, Sahadevan K, Leung H, Hamdy F, Whitaker HC and Neal DE: LYRIC/AEG-1 is targeted to different subcellular compartments by ubiquitinylation and intrinsic nuclear localization signals. Clin Cancer Res 15: 3003-3013, 2009.
3. Yoo BK, Emdad L, Lee SG, Su ZZ, Santhekadur P, Chen D, Gredler R, Fisher PB and Sarkar D: Astrocyte elevated gene-1 (AEG-1): A multifunctional regulator of normal and abnormal physiology. Pharmacol Ther 130: 1-8, 2011.
4. Emdad L, Sarksr D, Su ZZ, Randolph A, Boukerche H, Valerie K and Fisher PB: Activation of the nuclear factor kappaB pathway by astrocyte elevated gene-1: Implications for tumor progression and metastasis. Cancer Res 66: 1509-1516, 2006.
5. Emdad L, Sarkar D, Su ZZ, Lee SG, Kang DC, Bruce JN, Volsky DJ and Fisher PB: Astrocyte elevated gene-1: Recent insights into a novel gene involved in tumor progression, metastasis and neurodegeneration. Pharmacol Ther 114: 155-170, 2007.
6. Zhang C, Li HZ, Qian BJ, Liu CM, Guo F and Lin MC: MTDH/AEG-1-based DNA vaccine suppresses metastasis and enhances chemosensitivity to paclitaxel in pelvic lymph node metastasis. Biomed Pharmacother 70: 217-226, 2015.
7. Roussel BD, Kruppa AJ, Miranda E, Crowther DC, Lomas DA and Marciniak SJ: Endoplasmic reticulum dysfunction in neurological disease. Lancet Neurol 12: 105-118, 2013.
8. Anttila V, Stefansson H, Kallela M, Todt U, Terwindt GM, Calafato MS, Nyholt DR, Dimas AS, Freilinger T, Müller-Myhsok B, et al: Genome-wide association study of migraine implicates a common susceptibility variant on 8q22.1. Nat Genet 42: 869-873, 2010.
9. Kang DC, Su ZZ, Sarkar D, Emdad L, Volsky DJ and Fisher PB: Cloning and characterization of HIV-1-inducible astrocyte elevated gene-1, AEG-1. Gene 353: 8-15, 2005.
10. Lee SG, Kim K, Kegelman TP, Dash R, Das SK, Choi JK, Emdad L, Howlett EL, Jeon HY, Su ZZ, et al: Oncogene AEG-1 promotes glioma-induced neurodegeneration by increasing glutamate excitotoxicity. Cancer Res 71: 6514-6523, 2011.
11. Vartak-Sharma N and Ghorpade A: Astrocyte elevated gene-1 regulates astrocyte responses to neural injury: Implications for reactive astrogliosis and neurodegeneration. J Neuroinflammation 9: 195, 2012.
12. Yin X, Ren M, Jiang H, Cui S, Wang S, Jiang H, Qi Y, Wang J, Wang X, Dong G, et al: Downregulated AEG-1 together with inhibited PI3K/Akt pathway is associated with reduced viability of motor neurons in an ALS model. Mol Cell Neurosci 68: 303-313, 2015.
13. Leem E, Kim HJ, Choi M, Kim S, Oh YS, Lee KJ, Choe YS, Um JY, Shin WH, Jeong JY, et al: Upregulation of neuronal astrocyte elevated gene-1 protects nigral dopaminergic neurons in vivo. Cell Death Dis 9: 449, 2018.
14. Jeon HY, Choi M, Howlett EL, Vozhilla N, Yoo BK, Lloyd JA, Sarkar D, Lee SG and Fisher PB: Expression patterns of astrocyte elevated gene-1 (AEG-1) during development of the mouse embryo. Gene Expr Patterns 10: 361-367, 2010.
15. Carnemolla A, Fossale E, Agostoni E, Michelazzi S, Calligaris R, De Maso L, Del Sal G, MacDonald ME and Persichetti F: Rrs1 is involved in endoplasmic reticulum stress response in Huntington disease. J Biol Chem 284: 18167-18173, 2009.
16. Garneau JE, Dupuis MÈ, Villion M, Romero DA, Barrangou R, Boyaval P, Fremaux C, Horvath P, Magadán AH and Moineau S: The CRISPR/Cas bacterial immune system cleaves bacteriophage and plasmid DNA. Nature 468: 67-71, 2010.
17. Doudna JA and Charpentier E: Genome editing. The new frontier of genome engineering with CRISPR-Cas9. Science: Nov 28, 2014 (Epub ahead of print).
18. Caldwell JD, Shapiro RA, Jirikowski GF and Suleman F: Internalization of sex hormone-binding globulin into neurons and brain cells in vitro and in vivo. Neuroendocrinology 86: 84-93, 2007.
19. Murphy TH, Miyamoto M, Sastre A, Schnaar RL and Coyle JT: Glutamate toxicity in a neuronal cell line involves inhibition of cystine transport leading to oxidative stress. Neuron 2: 1547-1558, 1989.
20. Livak KJ and Schmittgen TD: Analysis of relative gene expression data using real-time quantitative PCR and the 2(-Delta Delta C(T)) method. Methods 25: 402-408, 2001.
21. Florea L, Song L and Salzberg SL: Thousands of exon skipping events differentiate among splicing patterns in sixteen human tissues. F1000Res 2: 188, 2013.
22. Robinson MD, McCarthy DJ and Smyth GK: edgeR: A bioconductor package for differential expression analysis of digital gene expression data. Bioinformatics 26: 139-140, 2010.
23. Anders S and Huber W: Differential expression analysis for sequence count data. Genome Biol 11: R106, 2010.
24. Benjamini Y and Hochberg Y: Controlling the false discovery rate: A practical and powerful approach to multiple testing. J R Stat Soc B (Methodol) 57: 289-300, 1995.
25. Harris MA, Clark J, Ireland A, Lomax J, Ashburner M, Foulger R, Eilbeck K, Lewis S, Marshall B, Mungall C, et al: The gene ontology (GO) database and informatics resource. Nucleic Acids Res 32: D258-D261, 2004.
26. Yu G, Wang LG, Han Y and He QY: clusterProfiler: An R package for comparing biological themes among gene clusters. OMICS 16: 284-287, 2012.
27. Kanehisa M, Sato Y, Kawashima M, Furumichi M and Tanabe M: KEGG as a reference resource for gene and protein annotation. Nucleic Acids Res 44: D457-D462, 2016.
28. von Mering C, Jensen LJ, Snel B, Hooper SD, Krupp M, Foglierini M, Jouffre N, Huynen MA and Bork P: STRING: Known and predicted protein-protein associations, integrated and transferred across organisms. Nucleic Acids Res 33: D433-D437, 2005.
29. Xu WH, Xu Y, Wang J, Wan FN, Wang HK, Cao DL, Shi GH, Qu YY, Zhang HL and Ye DW: Prognostic value and immune infiltration of novel signatures in clear cell renal cell carcinoma microenvironment. Aging (Albany NY) 11: 6999-7020, 2019.
30. Chen Q, Yu D, Zhao Y, Qiu J, Xie Y and Tao M: Screening and identification of hub genes in pancreatic cancer by integrated bioinformatics analysis. J Cell Biochem 120: 19496-19508, 2019.
31. Stephenson AA, Raper AT and Suo Z: Bidirectional degradation of DNA cleavage products catalyzed by CRISPR/Cas9. J Am Chem Soc 140: 3743-3750, 2018.
32. Bernardino L, Agasse F, Silva B, Ferreira R, Grade S and Malva JO: Tumor necrosis factor-alpha modulates survival, proliferation, and neuronal differentiation in neonatal subventricular zone cell cultures. Stem Cells 26: 2361-2371, 2008.
33. Li X, Bechara R, Zhao J, McGeachy MJ and Gaffen SL: IL-17 receptor-based signaling and implications for disease. Nat Immunol 20: 1594-1602, 2019.
34. Liu W, Ye J and Yan H: Investigation of key genes and pathways in inhibition of oxycodone on vincristine-induced microglia activation by using bioinformatics analysis. Dis Markers 2019: 3521746, 2019.
35. Ng SR, Rideout WM III, Akama-Garren EH, Bhutkar A, Mercer KL, Schenkel JM, Bronson RT and Jacks T: CRISPR-mediated modeling and functional validation of candidate tumor suppressor genes in small cell lung cancer. Proc Natl Acad Sci USA 117: 513-521, 2020.
36. He XY, Ren XH, Peng Y, Zhang JP, Ai SL, Liu BY, Xu C and Cheng SX: Aptamer/peptide-functionalized genome-editing system for effective immune restoration through reversal of PD-L1-mediated cancer immunosuppression. Adv Mater 32: 2000208, 2020.
37. Ling X, Xie B, Gao X, Chang L, Zheng W, Chen H, Huang Y, Tan L, Li M and Liu T: Improving the efficiency of precise genome editing with site-specific Cas9-oligonucleotide conjugates. Sci Adv 6: eaaz0051, 2020.
38. LaFountaine JS, Fathe K and Smyth HD: Delivery and therapeutic applications of gene editing technologies ZFNs, TALENs, and CRISPR/Cas9. Int J Pharm 494: 180-194, 2015.
39. Zhou Z, Tan H, Li Q, Chen J, Gao S, Wang Y, Chen W and Zhang L: CRISPR/Cas9-mediated efficient targeted mutagenesis of RAS in Salvia miltiorrhiza. Phytochemistry 148: 63-70, 2018.
40. Noch EK and Khalili K: The role of AEG-1/MTDH/LYRIC in the pathogenesis of central nervous system disease. Adv Cancer Res 120: 159-192, 2013.
41. Wang Y, Zhang W, Zhu X, Wang Y, Mao X, Xu X and Wang Y: Upregulation of AEG-1 involves in schwann cell proliferation and migration after sciatic nerve crush. J Mol Neurosci 60: 248-257, 2016.
42. Vartak-Sharma N, Nooka S and Ghorpade A: Astrocyte elevated gene-1 (AEG-1) and the A(E)Ging HIV/AIDS-HAND. Prog Neurobiol 157: 133-157, 2017.

43. Serviddio G, Romano AD, Cassano T, Bellanti F, Altomare E and Vendemiale G: Principles and therapeutic relevance for targeting mitochondria in aging and neurodegenerative diseases. Curr Pharm Des 17: 2036-2055, 2011.
44. Mohan H, Verhoog MB, Doreswamy KK, Eyal G, Aardse R, Lodder BN, Goriounova NA, Asamoah B, B Brakspear AB, Groot C, *et al*: Dendritic and axonal architecture of individual pyramidal neurons across layers of adult human neocortex. Cereb Cortex 25: 4839-4853, 2015.
45. Jan YN and Jan LY: Branching out: Mechanisms of dendritic arborization. Nat Rev Neurosci 11: 316-328, 2010.
46. Yoo BK, Emdad L, Su ZZ, Villanueva A, Chiang DY, Mukhopadhyay ND, Mills AS, Waxman S, Fisher RA, Llovet JM, *et al*: Astrocyte elevated gene-1 regulates hepatocellular carcinoma development and progression. J Clin Invest 119: 465-477, 2009.
47. Yu C, Chen K, Zheng H, Guo X, Jia W, Li M, Zeng M, Li J and Song L: Overexpression of astrocyte elevated gene-1 (AEG-1) is associated with esophageal squamous cell carcinoma (ESCC) progression and pathogenesis. Carcinogenesis 30: 894-901, 2009.
48. Lee SG, Su ZZ, Emdad L, Sarkar D and Fisher PB: Astrocyte elevated gene-1 (AEG-1) is a target gene of oncogenic Ha-ras requiring phosphatidylinositol 3-kinase and c-Myc. Proc Natl Acad Sci USA 103: 17390-17395, 2006.
49. Rohm B, Ottemeyer A, Lohrum M and Püschel AW: Plexin/neuropilin complexes mediate repulsion by the axonal guidance signal semaphorin 3A. Mech Dev 93: 95-104, 2000.
50. Rolny C, Capparuccia L, Casazza A, Mazzone M, Vallario A, Cignetti A, Medico E, Carmeliet P, Comoglio PM and Tamagnone L: The tumor suppressor semaphorin 3B triggers a prometastatic program mediated by interleukin 8 and the tumor microenvironment. J Exp Med 205: 1155-1171, 2008.
51. Mumm JS, Schroeter EH, Saxena MT, Griesemer A, Tian X, Pan DJ, Ray WJ and Kopan R: A ligand-induced extracellular cleavage regulates gamma-secretase-like proteolytic activation of Notch1. Mol Cell 5: 197-206, 2000.
52. Liu X, Yang Z, Yin Y and Deng X: Increased expression of Notch1 in temporal lobe epilepsy: Animal models and clinical evidence. Neural Regen Res 9: 526-533, 2014.
53. Feng S, Shi T, Qiu J, Yang H, Wu Y, Zhou W, Wang W and Wu H: Notch1 deficiency in postnatal neural progenitor cells in the dentate gyrus leads to emotional and cognitive impairment. FASEB J 31: 4347-4358, 2017.
54. Shu Y, Xiao B, Wu Q, Liu T, Du Y, Tang H, Chen S, Feng L, Long L and Li Y: The ephrin-A5/EphA4 interaction modulates neurogenesis and angiogenesis by the p-Akt and p-ERK pathways in a mouse model of TLE. Mol Neurobiol 53: 561-576, 2016.
55. Feng L, Shu Y, Wu Q, Liu T, Long H, Yang H, Li Y and Xiao B: EphA4 may contribute to microvessel remodeling in the hippocampal CA1 and CA3 areas in a mouse model of temporal lobe epilepsy. Mol Med Rep 15: 37-46, 2017.
56. Salińska E and Łazarewicz JW: Role of calcium in physiology and pathology of neurons. Postepy Biochem 58: 403-417, 2012 (In Polish).
57. Chadwick L, Gentle L, Strachan J and Layfield R: Review: Unchained maladie-a reassessment of the role of Ubb(+1)-capped polyubiquitin chains in Alzheimer's disease. Neuropathol Appl Neurobiol 38: 118-131, 2012.
58. Manavalan A, Mishra M, Feng L, Sze SK, Akatsu H and Heese K: Brain site-specific proteome changes in aging-related dementia. Exp Mol Med 45: e39, 2013.
59. Kothur K, Bandodkar S, Wienholt L, Chu S, Pope A, Gill D and Dale RC: Etiology is the key determinant of neuroinflammation in epilepsy: Elevation of cerebrospinal fluid cytokines and chemokines in febrile infection-related epilepsy syndrome and febrile status epilepticus. Epilepsia 60: 1678-1688, 2019.
60. Silva RL, Lopes AH, Guimaraes RM and Cunha TM: CXCL1/CXCR2 signaling in pathological pain: Role in peripheral and central sensitization. Neurobiol Dis 105: 109-116, 2017.
61. Ringland C, Schweig JE, Eisenbaum M, Paris D, Ait-Ghezala G, Mullan M, Crawford F, Abdullah L and Bachmeier C: MMP9 modulation improves specific neurobehavioral deficits in a mouse model of Alzheimer's disease. BMC Neurosci 22: 39, 2021.